The Effect of Lipid Oxidation on the Water Permeability of Phospholipid Bilayers

Mateusz Lis,[a,b] AlicjaWizert,[b]

Magda Przybylo,[b] Marek Langner,[b] Jerzy Swiatek [a], Pavel Jungwirth,[c] Lukasz Cwiklik [c,d*]

[a]*Institute of Information Science and Engineering, Faculty of Computer Science and Management, Wrocław University of Technology, Wyb. Wyspianskiego 27, Wroclaw, Poland*

[b]*Laboratory for Biophysics of Macromolecular Aggregates, Institute of Biomedical Engineering and Measurements, Wrocław University of Technology, Pl. Grunwaldzki 13, Wroclaw, Poland*

[c] *Institute of Organic Chemistry and Biochemistry, Academy of Sciences of the Czech Republic and Center for Biomolecules and Complex Molecular Systems, Flemingovo nám. 2, 16610 Prague 6, Czech Republic;*

[d] *J. Heyrovský Institute of Physical Chemistry, Academy of Sciences of the Czech Republic, v. v. i., Dolejškova 3, 18223 Prague 8, Czech Republic*

**email address: lukasz.cwiklik@uochb.cas.cz*

Abstract

The effect of lipid oxidation on water permeability of phosphatidylcholine membranes was investigated by means of both scattering stopped flow experiments and atomistic molecular dynamics simulations. Formation of water pores followed by a significant enhancement of water permeability was observed. The molecules of oxidized phospholipids facilitate pore formation and subsequently stabilize water in the membrane interior. A wide range of oxidation ratio, from 15 to 100 mol%, was considered. The degree of oxidation was found to strongly influence the time needed for the opening of a pore. The oxidation ratio of 75 mol% was found to be a threshold for spontaneous pore formation in the tens of nanosecond timescale, whereas 15 mol% of oxidation led to significant water permeation in the timescale of seconds. Once a pore was formed, the water permeability was found to be virtually independent on the oxidation ratio.

1. Introduction

Phospholipid bilayers are basic components of the majority of cellular membranes. Their principal role is to form a semipermeable barrier which separates the interior of a cell from the environment. Due to the amphiphilic character of phospholipid molecules the interior of the bilayer is hydrophobic while the membrane–water interface is predominantly occupied by hydrophilic polar headgroups of lipid molecules. The hydrophobic properties of the membrane interior result in low permeability of water, ions, and other polar molecules across the bilayer. As a consequence, the cross-membrane transport of polar moieties is usually an activated process which requires assistance of specialized protein-based transporters or ion channels.[1] However,

the unassisted transport of polar groups (ions, polypeptides, and lipids) was reported in various experiments,[2-4] and was recently a subject of several computational studies.[5-7] According to the molecular dynamics (MD) simulations, the unassisted transport is usually accompanied by formation of trans-membrane water pores.[7] Each water pore creates a localized polar environment in the membrane interior and thus facilitates the transport of hydrophilic species across the bilayer. Under typical conditions, formation of pores is a rare event and the membrane interior is highly dehydrated, as confirmed by recent neutron diffraction experiments.[8] Nevertheless, permeation of water and creation of pores can be enhanced in several ways. For example, as shown both experimentally[9] and in MD simulations,[10] the presence of electric field acting across a bilayer enhances the probability of pore creation. A special case of this phenomenon is formation of pores due to concentration gradients of ions on both sides of a bilayer.[5] Mechanical factors, for instance, osmotic stress, are also known to promote pore formation.[10] Similarly, a presence of some surfactants facilitates creation of pores.[6]

Oxidation of phospholipid molecules in the membrane is another factor which can facilitate creation of pores.[11] This phenomenon seems to be particularly important from the physiological point of view. Cell membranes are composed of both saturated and unsaturated lipids. The presence of double bonds, typically in the *cis*-configuration, is responsible for reduced melting temperature and increased fluidity with respect to a fully-saturated bilayer. At the same time, the double bonds in the acyl chains of unsaturated phospholipids are prone to oxidative processes; in particular to a non-specific oxidation caused by reactive oxygen species.[12] These reactions usually cause the cleavage of unsaturated acyl chains and introduce polar moieties at their terminals.[13] The modified chains reorient in such a way that the polar groups are transferred from the hydrophobic interior of the bilayer toward the headgroups, or even to the water phase.[14, 15]

The structural changes influence the hydration of a bilayer. According to MD simulations, oxidation results in both the membrane thickening and the increase of the area per lipid; moreover, the free energy of water transfer across the bilayer is reduced.[16] Indeed, fluorescence spectroscopy experiments indicate that hydration of oxidized bilayers at the glycerol level is enhanced.[17] More interestingly, recent studies suggest that oxidation may cause creation of transmembrane pores. This was shown by means of neutron scattering[18] and fluorescence spectroscopy;[19] and was further confirmed in our previous MD study.[11]

In the present work we investigate the effect of lipid oxidation on the water permeability of phospholipid membranes built of phosphatidylcholine (PC) lipids employing both scattering stopped flow experiments and MD simulations. In particular, we focus on the influence of the extent of oxidation on water permeation, and on the process of pores formation. In the stopped flow experiments we measure the efflux of water from phospholipid eggPC vesicles containing various amounts of oxidized lipids. This is accompanied by MD simulations of model oxidized PC membranes in which we aim at assessing the threshold for opening of pores, and the role of oxidized lipids in this process.

2. Experimental methods

2.1 Chemicals and liposome preparation

Oxidized lipid, POVPC, (1-palmitoyl-2-(5'-oxo-valeroyl)-*sn*-glycero-3-phosphocholine) , eggPC (egg phosphatidylcholine) as well as DOPC (18:1 (Δ9-Cis) PC, 1,2-dioleoyl-*sn*-glycero-3-phosphocholine) were purchased from Avanti Lipids (Netherlands, Amsterdam) and were of analytical grade. Experiments were carried out in distilled water (conductivity 2μS). In order to

generate the osmotic pressure difference the water solution of KCl (POCH, Poland, 99.99%) was used. Liposomes were prepared by the extrusion method, described in details elsewhere [20]. In short, the appropriate amounts of lipids dissolved in chloroform were mixed together and the organic solvent was removed under the stream of nitrogen. To remove the remnants of the solvent the initially obtained dry lipid film was left overnight under vacuum. Next, the obtained lipid film was hydrated with distilled water and the resulting multilamellar vesicles solution was then extruder through 100 nm polycarbonate membrane filters (Whatmann, NanoPore). The size distributions of such liposome solution were analyzed using the dynamic light scattering technique (Malvern, England).

2.2 Scattering Stopped Flow experiments

The kinetics of osmotically-induced water flow was measured by means of stopped-flow technique, where the light scattering as a function of time was recorded at the angle of 90° to the incident light. The wavelength of the incident beam was set to 405 nm. The instrument (BioLogic, Grenoble France) was equipped with a xenon-mercury lamp, a monochromator with the 0.5 nm slit, and a quartz flow cuvette of 15 mm optical path length. The liposome suspension in water (~ 0 mOsm) was mixed with the potassium chloride solution of different osmolality (30, 100, or 300 mOsm) in a 1 to 1 volume ratio, producing the desired osmotic pressure across the liposome membrane (15, 50, or 150 mOsm).

2.3 Experimental design

In order to measure the water efflux we applied a modified stopped-flow approach, similar to presented by Mathai et. al [21], where the water flow under the different (15-150 mOsm) hypertonic conditions is evaluated. To study thoroughly the effect of the osmotic pressure

difference on the membrane permeability we have simplified the experimental system in such a way that the water flux was directed out of the vesicle and the intra-vesicle osmotic pressure was chosen to be zero so there is no intra-vesicle concentration buildup. Consequently, the osmotic pressure difference should remain constant regardless on the volume of the intra-vesicle aqueous phase. This ensures the constant water flow through the lipid bilayer, assuming that the surface area of the membrane will not change. In such case the water flow should follow the simple relation[22] :

$$\frac{dV}{V_w A dt} = \frac{P\Delta\pi}{RT} \quad (1)$$

where A represents the vesicle surface area, P membrane permeability, V_w the molar volume of water, and $\Delta\pi_t$ the osmotic pressure difference across the vesicle membrane. According to this equation the water flux should remain constant and consequently the observed kinetic should have a form of a straight line with the slope proportional to the salt concentration outside the vesicle and to the membrane permeability coefficient. Examples of experimentally determined kinetics collected for a series of osmotic pressure differences for vesicles formed from egg-PC are presented in Fig. 1. Curves presented show that for all employed osmotic pressure differences the intensity of light scattering is not a linear function of time as predicted by the Equation 1, however the numerical values of slopes correlate with the osmotic pressure differences. The leveling of curve observed for longer times is likely a result of the balance between the membrane thermal fluctuations and/or its mechanical resilience to deformation at the condition when a large fraction of entrapped water already have flown out of vesicles. When curves are analyzed in short times, for all osmotic pressure differences the initial decrease of the scattered light intensity is followed by the interval where the light scattering rises linearly with time.

Finally, at longer times, curves change their character and monotonically approach levels of their final values of scattered light intensities. The complex shape of the kinetic curve reveals different states in the lipid membrane system, induced by the water outflow. To study quantitatively the effect of various extrinsic (osmotic pressure difference) and intrinsic (lipid bilayer composition) factors on the shape of the scattered light kinetics the curve was arbitrary sectioned into three distinct stages, as illustrated in Fig. 2. These stages were then parameterized so the quantitative comparison of different membranes would be possible. We postulate that during the initial stage (I) transient water filled trans-membrane pores are formed but there are not yet open. They will facilitate the subsequent water flow in the stage II. The probability of a pore opening should correlate with the reciprocal of the time t_0 (Fig. 2) and should depend on both intrinsic (lipid molecules composition) [21, 23-26] and extrinsic (electroporation or osmotic pressure difference [27-29]) factors.

3. Computational methods

Classical molecular dynamics simulations were performed employing the united atom Berger's force-field[30] for lipid molecules combined with the SPC potential[31] for water. Parameters for the aldehyde group of oxidized lipids were taken from Ref.[16] A previously equilibrated (>100 ns) bilayer consisting of 128 molecules of 1,2-dioleoyl-sn-glycero-3-phosphocholine (DOPC) lipid, 64 in each leaflet, was taken from our previous study.[11] Oxidation was performed by a cleavage of a given number (the same in each leaflet) of randomly chosen DOPC lipids, with the cleavage site located at the position of the double bond in the *sn-1* acyl chain. The $–CH_2$ groups at the cleavage site of both the lipid molecule and the remaining hydrocarbon chain were exchanged with aldehyde groups. As a result, a pair of a molecule of oxidized 1-(9'-oxo-nonanoyl)-2-oleoyl-sn-glycero-3-phosphocholine (OX1PC) accompanied

with a nonanal molecule was generated in the position of each oxidized DOPC molecule (see the reaction scheme in Fig. 1S in the Supplementary Material). Seven bilayers, with oxidation ratios in the range from 15 mol% to 90 mol% were considered (the exact composition of each system is given in Table 1S in the Supplementary Material). The bilayer from our previous study with 100 mol% of oxidation was also considered for comparison.[11] Each membrane was hydrated with 4810 molecules of water which resulted in the initial size of the simulation box of approximately $6.5\times6.5\times7.4$ nm^3. Number of water molecules was chosen in order to ensure full hydration of the bilayer, with the water/lipid ratio well above the experimental value of 32.5.[32] Each system was simulated for at least 100 ns; the time-averaged properties were calculated over the last 20 ns of the trajectories. Periodic boundary conditions were employed. Simulations were performed using the isothermal-isobaric ensemble. The pressure of 1 bar was controlled employing the semi-isotropic Parrinello-Rahman coupling scheme (coupling constant τ_p = 2 ps),[33] and the Nose-Hoover thermostat was employed (τ_T = 1ps), separately for lipids and water, with the temperature of 310 K. Non-bonding interactions were treated with a cutoff of 1 nm. The Particle-Mesh-Ewald scheme,[34] with a grid spacing of 0.12 nm and the fourth-order interpolation, was employed to account for long-range electrostatic forces. Water molecules were constrained employing the SETTLE algorithm,[35] and the bonds of remaining molecules were constrained with the LINCS scheme.[36] Calculations were performed using GROMACS 4.0.7 (double precision) software suite.[37]

4. Results and Discussion

Stopped-flow experiments

In the stopped-flow experiments the kinetics of water efflux from liposome were measured as a function of the membrane composition in the presence of 15 mol% and 30 mol% oxidized lipids (POVPC). The obtained kinetics showed two distinct time–separated processes reflecting different membrane properties. As has been discussed in the "Experimental design" section, the water flux through the lipid bilayer depends on two processes; the transient pore formation and the subsequent water flow. Following the pore opening the vesicle volume changes in two qualitatively different manners; the initial linear rise of the scattered light intensity followed by the slower change when sample approaches the maximal signal value. The first process reflects the osmotically induced water efflux, where the slope of the linear part of the kinetic is proportional to the water membrane permeability and osmotic pressure difference according to equation (1). As seen in Fig. 3 the presence of POVPC changes qualitatively the vesicle shrinking kinetics. The water flux (dV/dt) calculated from the initial rise of the light scattering dependence on time as a function of the osmotic pressure difference is presented in Fig. 4. It can be seen that the addition of the oxidized lipid increases water flux for all osmotic pressure differences used showing that the lipid bilayer permeability for water increases. Specifically, when the fraction of oxidized lipids in the membrane reaches 30 mol% the water permeability increases noticeable (by about 15 %) (see Fig. 2S in the Supplementary Material). As postulated earlier, the water flux, when the transmembrane pore is opened, depends only on the pore stability and its capacity to maintain the water flow. The results presented in Fig. 4 demonstrate the extended water flow at the presence of oxidized lipids. This is expected for lipids without or with shortened acyl chain in the sn-2 position, which are known for stabilizing the transmembrane pores.[38] As mentioned before, the membrane water permeability is affected by two factors; the probability of the opening of the hydrophilic pore and the extent of water flow

through the existing pore. The probability of pore opening can be directly connected with experimentally derived time t_0.[39] This is the time at which the linear increase of the scattered light starts, which indicates the pore formation and the water flow. As evident from Fig. 5 for each lipid bilayer the time t_0 depends on the reciprocal of the osmotic pressure difference. The dependence of the time t_0 on the extent of oxidation is evident from Fig. 5; the time t_0 as a function of oxidation ratio was also depicted in Fig. 3S in the Supplementary Material. It can be concluded that the content of the oxidized lipid influences the time t_0 and the water flow through an already opened pore in a somehow different way. Namely, 15 mol% of POVPC content has already a strong effect on the pore opening probability, as evident from the difference between the non-oxidized and the two oxidized membranes in Fig. 5 and S3. Further increase of oxidized lipid content, from 15 to 30 mol%, has much smaller effect. On the other hand, the alterations of water fluxes through already open pores are not so significant in the range of 0-15 mol% of oxidation, as evident from Fig. 4 and 2S. The flux increases considerably only upon an increase of oxidation content to 30 mol%.

The results obtained for eggPC lipids reveal the same characteristic as vesicles build of DOPC. The water flux, as well as the t_0 parameter behave in a similar way for both lipids (see Fig. 4S in the Supplementary Material). This lack of major differences in behavior of eggPC and DOPC is important since in the present study the molecular dynamics simulations were performed for model DOPC bilayers.

Molecular dynamics simulations

A) Structural changes in membranes upon oxidation

The presence of the products of lipid oxidation influences the structural properties of the DOPC membrane. In Fig. 6 the values of both the area per lipid (APL) and the membrane thickness upon equilibration are presented (for the time dependence of APL see Fig. 5S in the Supplementary Material). It is evident that the APL increases with the increasing content of oxidized lipids in the membrane. For the lowest oxidation level (15 mol%) a relatively small increase of the APL occurs, to approximately 0.71 nm^2, with regard to the value of 0.68 nm^2, as calculated for a pure-DOPC membrane in the previous study[11]. It should be noted, that the corresponding experimental APL for the DOPC membrane[40] equals to 0.721 nm^2 at 303 K; the small discrepancy between the experimental and the calculated value results from the approximations introduced in the classical force-field. In the case of 50 mol% oxidation, the APL increases and stabilizes at approximately 0.80 nm^2 which is significantly above the value calculated for the pure-POPC system. As the oxidation ratio increases above the value of 50%, the observed changes in the membrane structure become more significant as the values of APL rise above 0.80 nm^2. The increased values of the APL in oxidized membranes were also observed in previous computational studies of oxidized bilayers for both moderately[15, 16] and massively oxidized systems.[11] The lateral swelling of the membrane is accompanied by the decrease of membrane's thickness. As evident from Fig. 6, the thickness of the membrane decreases from approximately 3.6 nm for 15% of oxidation to the value of about 3.0 nm for the oxidation ratio in a range of 50–66%. This is in accord with previous computational studies regarding moderately oxidized lipid bilayers.[16] In the case of the massively oxidized systems (>66%), the thickness increases again, toward the values in a range of 3.2–3.4 nm. This increase of the thickness is most probably caused by the swelling of the membrane due to the presence of

water in the previously hydrophobic regions of the bilayer and by the resulting water permeation across the membrane.

The structural changes across the membrane can be further analyzed by means of the electron density profiles which are depicted in Fig. 7. In the initial stage of simulations (Fig. 7A) minor differences between the simulated systems occur. Namely, as the oxidation ratio increases the peaks of the electron density shrink and their maxima are shifted toward the membrane interior. Moreover, the electron density in the membrane interior increases. In the final stages of the trajectories (Fig. 7B) no significant changes with regard to the earlier stages of simulations can be observed for the moderately oxidized systems. On the contrary, for strongly oxidized membranes (>50 mol%) the changes are profound: the maxima of the density profiles are diminished significantly, and the density in the membrane interior increases considerably when compared to the beginning of the trajectories.

The visual analysis of the simulation boxes revealed that for the oxidation ratio in a range of 15–66% the general structure of the membrane was maintained, and no significant penetration of the bilayer by water was observed during simulation (results not shown). Water defects, in a form of water clusters, were formed in the headgroup region; however, these defects had a transient character. On the contrary, in the case of a high oxidation ratios (75–100%) the penetration of water into the headgroup region of the bilayer occurred already in the initial stages of each trajectory; relatively large water defects were formed, and water molecules were stabilized in the polar region of the bilayer. In the later stages of simulations some of these water defects formed trans-membrane pores filled with water. A representative example of such process is depicted in Fig. 8. In the snapshot taken at 10 ns from the beginning of the simulation the water defects in the headgroup region are present; these defects further evolve and form

trans-membrane which is apparent in the snapshot taken at 90 ns. The structural changes in the membrane upon oxidation predicted in molcular simulations are in qualitative agreement with experimental measurements, which show the increased water permeability of oxidized bilayers.

B) The mechanism of pore formation

Formation of relatively large water defects in the headgroup region is feasible due to increased distances between the headgroups. As evident based on the increase of the area per lipid (Fig. 6), an average inter-lipid distance increases upon oxidation. This behavior can be further analyzed by means of radial distribution functions, g(r), calculated for phosphate atoms of lipid headgroups. The radial distribution functions, for both initial and final stages of simulations for selected systems are presented in Fig. 9. An extent of the changes occurring in the headgroup–headgroup structure depends on the oxidation level. In the case of 15% of oxidation only minor variations of g(r) are present. As the oxidation ratio increases, the changes are more pronounced, and are apparent even in the initial stages of simulations, see Fig. 9A. The values of the maxima of g(r) decrease with respect to the least oxidized system. Surprisingly, the location of the maxima virtually does not vary as the oxidation rate grows; even though the area per lipid increases under these conditions (compare with Fig. 6). This behavior can be rationalized taking into account formation of water defects in the region of lipid headgroups. As water penetrates and the defects are formed, the membrane swells, and the area per lipid increases. However, the average distance between the headgroups is almost not changed, as the peaks of g(r) are located at the same position. Hence, it indicates that some sort of separation between water and headgroups takes place. Such separation occurs most likely due to formation

of water cluster which can be views as “water islands” at the membrane’s surface. At the same time, the regions outside of these water defects are occupied by lipids, and have the structure mostly unchanged with the respect to the non-oxidized membrane. As simulation continues, hydration of the headgroup region increases and induces further diminish of the maxima of g(r), as presented in Fig. 9B.

On top of the abovementioned enhance of water penetration due to the non-specific increase of the lipid-lipid distances there are specific factors which facilitate water defects and which originate from the hydrophilic character of oxidation products. In the oxidized bilayer the polar moieties, in our case the –CHO groups that terminate both the oxidized chain of ox-DOPC molecules as well as the nonanal chains, are introduced in the originally hydrophobic membrane interior. These groups are hydrophilic; hence, they tend to migrate toward the water phase.[14, 15, 17] In the case of nonanal, the reorientation has a minor influence on the membrane properties, as nonanal molecules are relatively small and are able to accommodate between the lipid molecules upon reorientation. However, in the case of relatively large molecules of the oxidized lipid the reorientation process is more complex. Firstly, only the oxidized chains reorient toward the water phase, the non-oxidized purely hydrocarbon chains remain mostly in the original orientation. This behavior is illustrated in Fig. 10, where the distribution of angles between the oxidized chains of lipids and the membrane normal is presented. Results for both 50% and 75% oxidation ratio are shown. In the former case the oxidized lipid chains do not reorient significantly in the course of simulation; they point mostly toward the membrane interior (the angle distribution concentrates between 0° and 90°). In the case of 75 mol% oxidation, the reorientation of oxidized chains in the simulation timescale is evident; in the initial stages of the trajectory the orientation towards the membrane interior dominates (the distribution between 0° and 90°),

whereas after ~90 ns a non-negligible fraction of oxidized chains points toward the water phase (non-zero distribution between 90° and 180°). It should be stressed, that for the oxidation ratio of 75% this reorientation is not complete, i.e., most of the oxidized chains preserve their "canonical" orientation and point toward the water phase after 100 ns of simulation. Moreover, the chain reorientation is not complete even for a entirely oxidized bilayer, as shown in our previous study.[11] Note, that the non-oxidized chains of oxidized lipids do not undergo significant reorientation; the angle distribution in their case is accumulated close to 0° (results not shown here). The reorientation of oxidized lipid chains for moderately oxidized membranes was previously reported in both theoretical and experimental studies.[14, 16] Reorientation of oxidized lipid chains has two consequences for water permeability. Firstly, it results in creation of voids in the membrane which can be filled with water, as described in our previous work.[17] Secondly, as this reorientation is not complete, water has a tendency to penetrate toward the completely reoriented –CHO groups. These both factors result in the increased hydration of the membrane, followed in some cases by formation of water defects and pores.

The final stages of a representative pore formation process are illustrated in Fig. 8, as well as in Fig. 6S in the Supporting Material. The water defects are formed in the vicinity of the oxidized lipid molecule which has a reoriented oxidized chain. The polar –CHO moiety moves toward the water phase and, at the same location, penetration of water molecules toward the headgroup region is enhanced. Some of the water molecules bind even with the deeper-located carbonyl groups of the oxidized molecule. It is well established that carbonyl groups in phospholipid membranes are hydrated to a certain extent but the presence of extra polar groups in oxidized membranes enhances the membrane's hydration.[17] Most of the observed water defects were transient; however, some of them persisted in the timescale of tens of nanoseconds,

and subsequently formed water pores. The penetration of water molecules through the membrane interior which follows the water defect is facilitated by the presence of not fully reoriented polar –CHO groups. This is evident from the presence of –CHO groups at the surface of water pore, as depicted in Fig. 6S. Thus the transmembrane pore is stabilized by molecules of the oxidized lipid. The walls of the pore are formed by the headgroups of reoriented lipid molecules, as well as polar –CHO groups. The atomistic-level description of pore formation is not accessible for the osmotic pressure measurements employed in the present work. Nevertheless, the opening of pores in oxidized membranes demonstrated in molecular dynamics simulations corroborates the leakage results obtained in experimental part of this study.

C) The extent of water permeation

We observed that formation of pores is strongly dependent on the extent of membrane oxidation; moreover, the form of the created pore varies. Namely, in the case of moderately oxidized membranes (15–30% of oxidation) a weak penetration of water, in a form of single water molecules diffusing across the bilayer, occurs. As oxidation ratio increases (55–66%), water clusters, which are formed by few water molecules, are typically transferred across the membrane. For larger extent of oxidation (66 mol%), we observed formation of transient chains formed by hydrogen-bonded water molecules, spanning across the bilayer. Eventually, in the case of the highest oxidation ratios (75–100 mol%) trans-membrane water pores were formed. We quantitatively studied the membrane's permeability and the transfer of water across the bilayer by means of a number of water molecules crossing the membrane during simulation. The corresponding results are presented in Fig. 11. Number of water molecules which crossed the

center of the bilayer is reported. For membranes with the low oxidation ratio ≤66 mol% the overall permeation is relatively low; the number of water molecules crossing the bilayer during 100 ns was between 9 and 43. As evident from Fig. 11A, water permeation across the bilayer in these systems starts already in the initial stages of the trajectory, and no significant changes in permeability with time occur. The character of water permeation changes significantly when oxidation ratio increases (≥75 mol%); both quantitative and qualitative differences occur (see Fig. 11B). Most importantly, the overall number of water molecules crossing the membrane is higher by two orders of magnitude with respect to the less oxidized systems. Moreover, permeability varies with time. In beginning of the trajectories, the permeation of water is moderate because no pores are present in the membrane. Subsequently, the pore is formed; and the time needed for opening of a pore varies with the oxidation ratio, from 3.0 to 9.2 ns for 75 mol% and 100 mol% of oxidation, respectively. As soon as a pore is open, extensive water permeation occurs. In two cases (90 and 100% of oxidation) the initially-formed pore was annihilated; however, a subsequent stable one was formed. In one case (75% of oxidation) the initially-formed pore survived till the end of the simulation. The enhancement of water permeability with increased level of oxidation is in accord with experimental results discussed beforehand. Moreover, the lack of significant alternations of water flux across the already opened pores was observed both in simulations and in experiments.

5. Discussion and conclusions

The present MD simulations allow us to make a specific distinction among the simulated systems based on their properties with regard to the pure-DOPC bilayer. The considered bilayers

can be divided into two groups: moderately oxidized (15–66 mol%), and massively oxidized (75–100 mol%). In the case of the moderate oxidation the changes in bilayer's properties were similar to those previously described in the literature.[15, 16] Namely, the reorientation of the polar groups of the oxidized lipid molecules resulted in the increase of the average lipid-lipid lateral distance. As a consequence, penetration of water molecules toward the region of headgroups was increased, and water defects were formed. However, at the moderate oxidation levels, water permeability across the bilayer was not significantly enhanced. As the oxidation ratio increases to 75%, qualitative changes in the membrane are observed. In the timescale of tens of nanoseconds trans-membrane water pores are created. Water permeation is moderate until the opening of a pore; and a significant penetration of water across the membrane is observed upon pore creation. Interestingly, the time needed for the opening of the pore is dependent on the oxidation ratio; in contrast, the extent of water permeation across the pore is virtually independent on the oxidation level. Some of the pores formed upon oxidation are transient in the timescale of simulations as a pore closing and re-opening was observed. The influence of the oxidized lipids on water permeability in the case of massively oxidized bilayers is two-fold. Firstly, the structural changes due to reorientation of oxidized chains promote penetration of water toward the membrane interior, which results in the opening of pores. Secondly, the presence of polar groups, in both oxidized lipids and short-chain aldehyde molecules, stabilizes the pore by hydrogen bonds formed between these groups and water in the membrane interior.

A comparison between the experimental and computational results is not straightforward due to the different time- and size-scales studied employing both methods. In simulations only the short timescales, up to hundreds of nanoseconds are accessible; however, the high oxidation can be studied to facilitate the changes in the system. In experiments the high oxidation ratios are

inaccessible since the highly-oxidized vesicles become unstable in the experimental timescale. Thus in the stopped flow experiments the permeation across the moderately oxidized membranes of macroscopic vesicles was investigated under the osmotic pressure in the timescale of minutes. In MD simulations, the microscopic bilayers were studied in the tens of nanoseconds timescales in a wide range of oxidation ratios. Nevertheless, combination of both techniques allows us to draw some general conclusions. Permeation of water across the studied phospholipid bilayers is significantly enhanced upon introduction of oxidized lipids. This process is connected with the opening of transmembrane pores. The time needed for the opening of a pore, although the different timescales were studied, is significantly shortened as the oxidation level increases. When pores are forms, not significant changes in the water permeation are observed.

The efficiency of transient pores formation in the lipid bilayers may have a far reaching consequences wherever lipids play a permeability barrier functions. In biological systems, where lipid bilayer is a basic structural element, the generation and maintenance of electrochemical potentials gradients, for both water and membrane soluble compounds, relies on the lipid bilayer integrity.[41] Membrane barriers make possible the generation of intracellular ionic homeostasis which depends, among other thing, on the efficient water flow, so any osmotic pressure differences across biological membranes, generated as a result of various metabolic processes, can be effectively eliminated.[42-47] Transient pores in the lipid bilayer will facilitate sufficient water flow in normal circumstances however, when drastic osmotic pressure differences are present the continuous nonspecific pore opening will compromise the membrane barrier functions as well as the lipid asymmetry.[48-51] In such a case the water specific aquaporins are present in large numbers so the amount of transient unspecific water pores can be reduced.[52] Therefore, the elevated probability of transient pore formation due to intrinsic factor, i.e. lipid

oxidation, as shown in this paper, may affect the intracellular homeostasis and/or the energetic requirements for their maintenance what will surely reduce the cell metabolic efficiency.[45] The effect of oxidized lipids on the membrane water permeability is also a critical factor in designing lipid based targeted drug delivery systems. In this case the control of lipid oxidation is necessary, not only for ensuring the stability of the chemical composition, but also maintaining the physicochemical properties of the preparation. The biologically active compounds encapsulation in lipid nano-capsules (liposomes) is a decisive factor affecting the drug targeting and extend of the undesired side effects. [53-59]

Acknowledgments

PJ and LC acknowledge the support of the Czech Science Foundation (EUROMEMBRANES project MEM/09/E006). PJ thanks the Academy of Sciences of the Czech Republic for support via Praemium Academie grant.

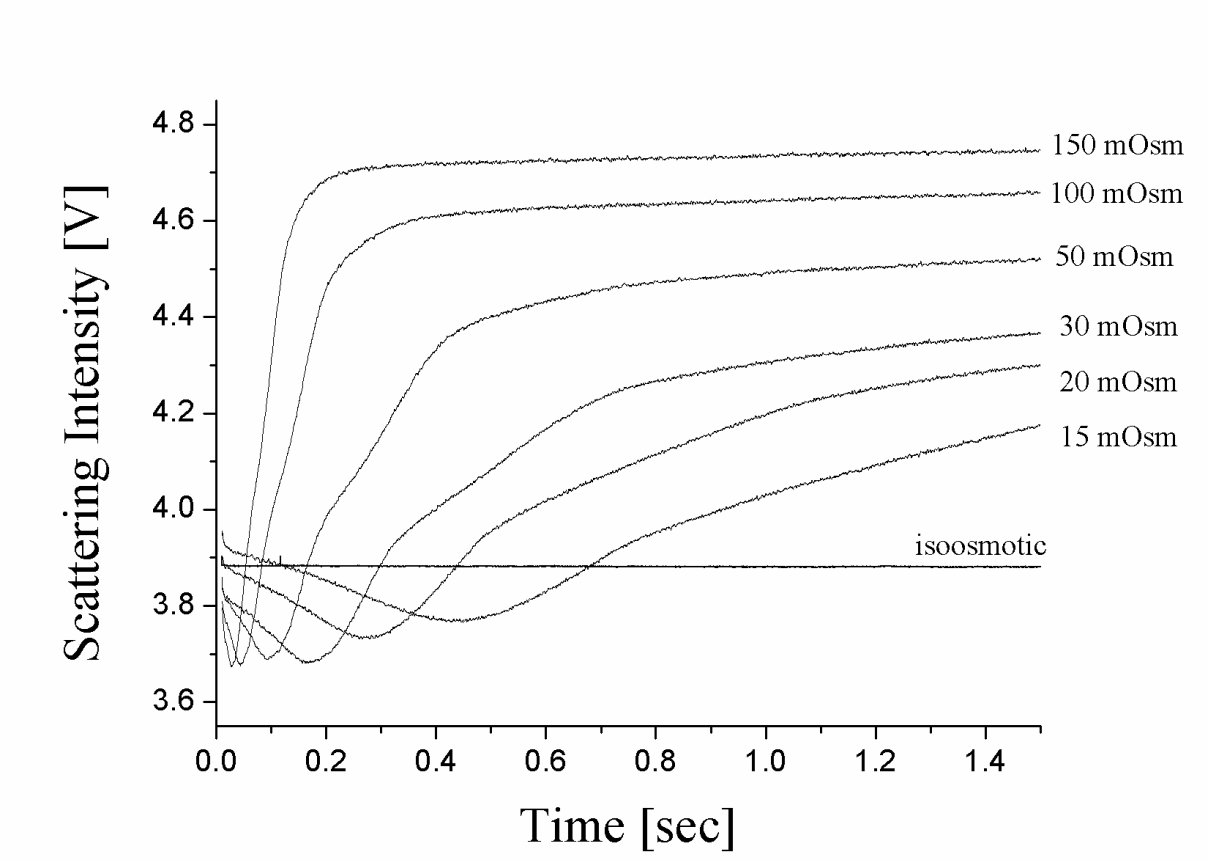

Figure 1. Light scattering kinetics of Egg-PC liposomes exposed to various osmotic pressure differences, collected shortly after vesicle suspension had been mixed with KCl solution. The straight horizontal line was obtained at an iso-osmotic condition indicating the intensity level of the scattered light when vesicles are invariant with time.

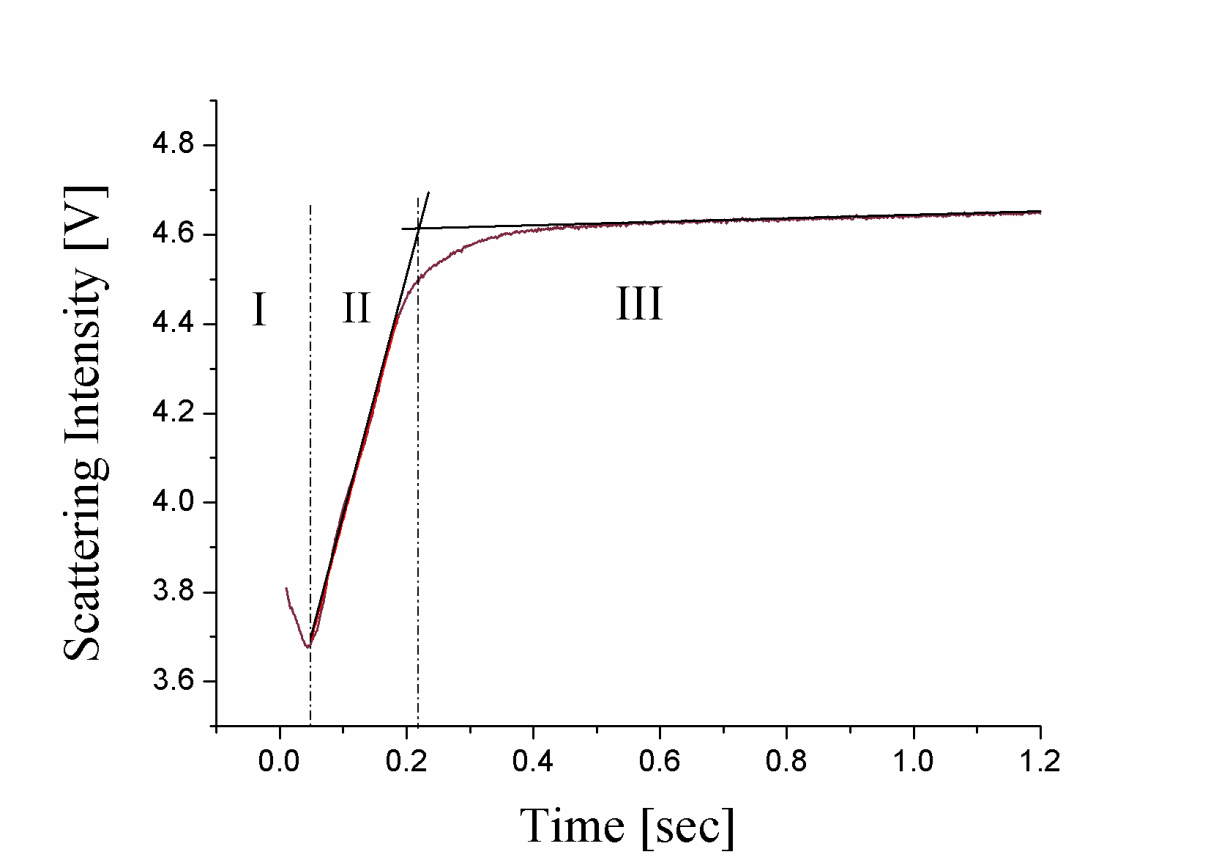

Figure 2 The illustration of the vesicle shrinkage kinetics and their division into three sections (Panel A); the decrease of a light scattering intensity (section I), its linear rise (section II) and the final part where scattered light increase rate decreases (section III). The parameterization of liposome shrinkage kinetics was achieved by selecting the average slope determined from section II and the duration of the initial intensity decrease (t_0) in section I (Panel B).

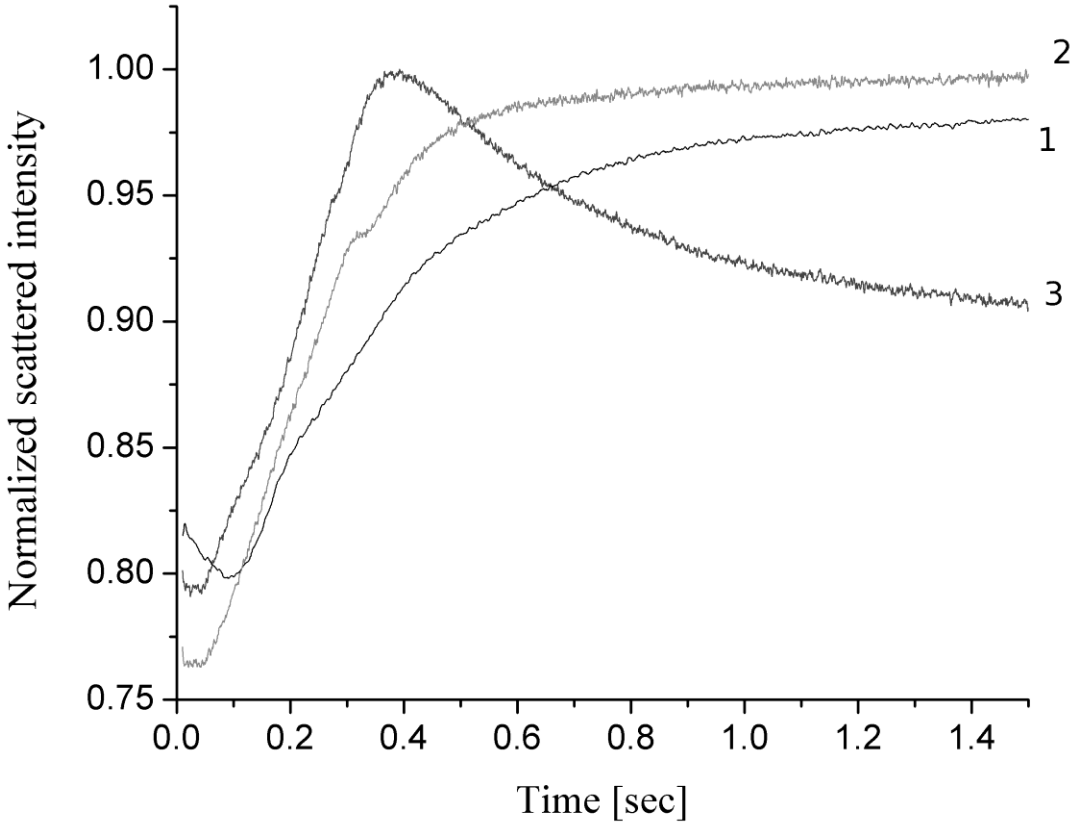

Figure 3. The kinetics of water efflux at 50 mOsm pressure difference for the following liposome compositions: eggPC (curve 1), eggPC:POVPC (85:15) (curve 2) and eggPC:POVPC (70:30) (curve 3). The shortening of the time required for a pore to open, at the presence of the oxidized lipids, can be determined during the first 100 milliseconds. The normalized scattered intensity is the ratio of the instantaneous measured scattered intensity to the maximum intensity measured during a single kinetic trace.

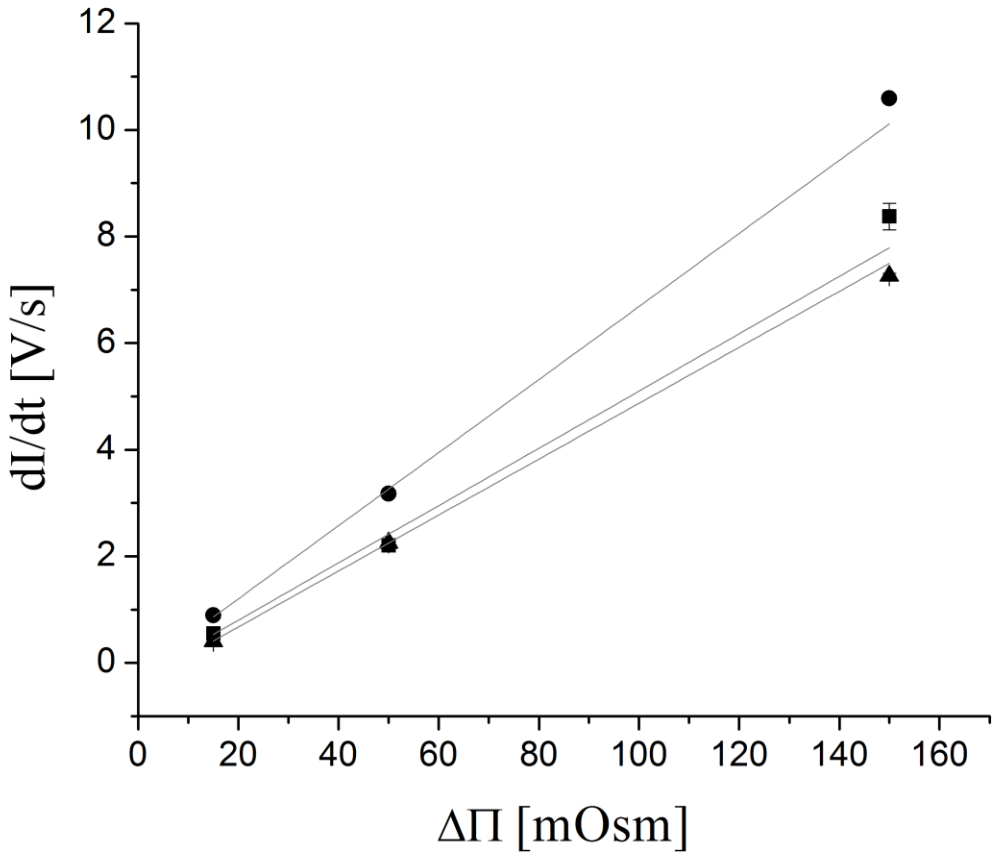

Figure 4. The determined scattered light change in time as a function of the osmotic pressure difference, indicating the water flux, for eggPC (■), eggPC:POVPC (85:15) (▲) and eggPC:POVPC (70:30) (●) is demonstrated.

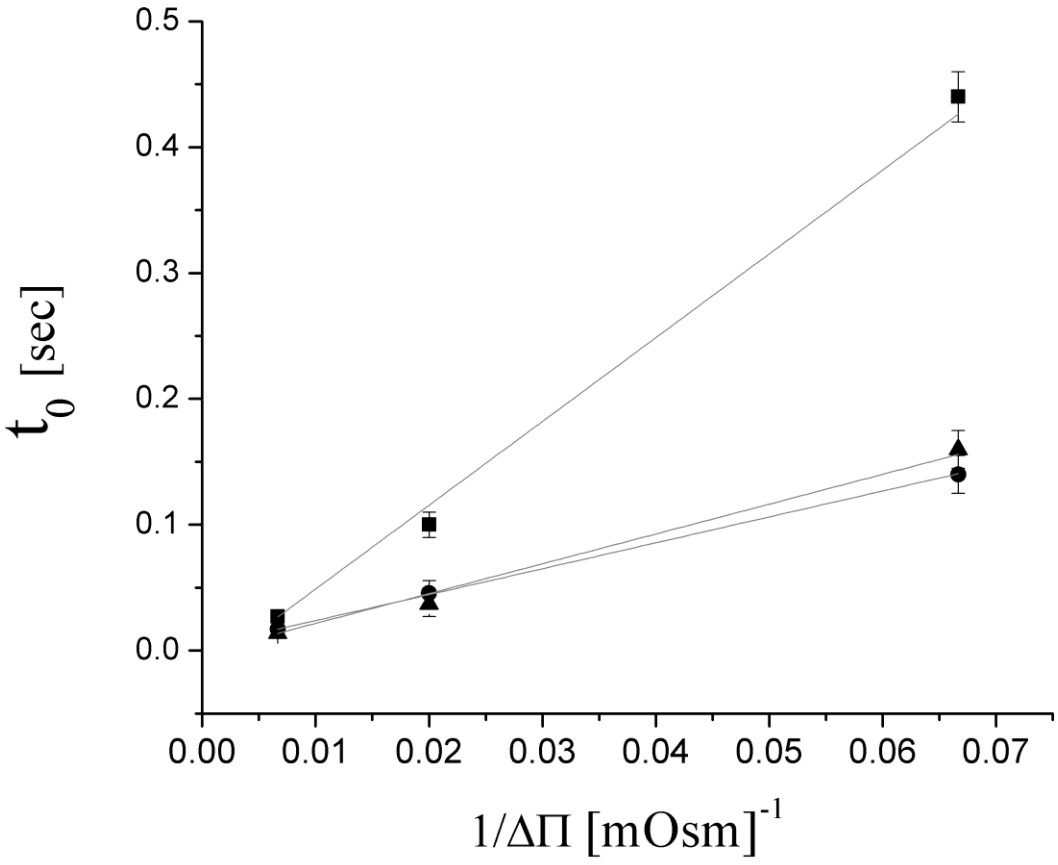

Figure 5. The initial time (t_0), correlated with pore opening as the function of the osmotic pressure difference, for eggPC (■), eggPC:POVPC (85:15) (▲) and eggPC:POVPC (70:30) (●) is shown.

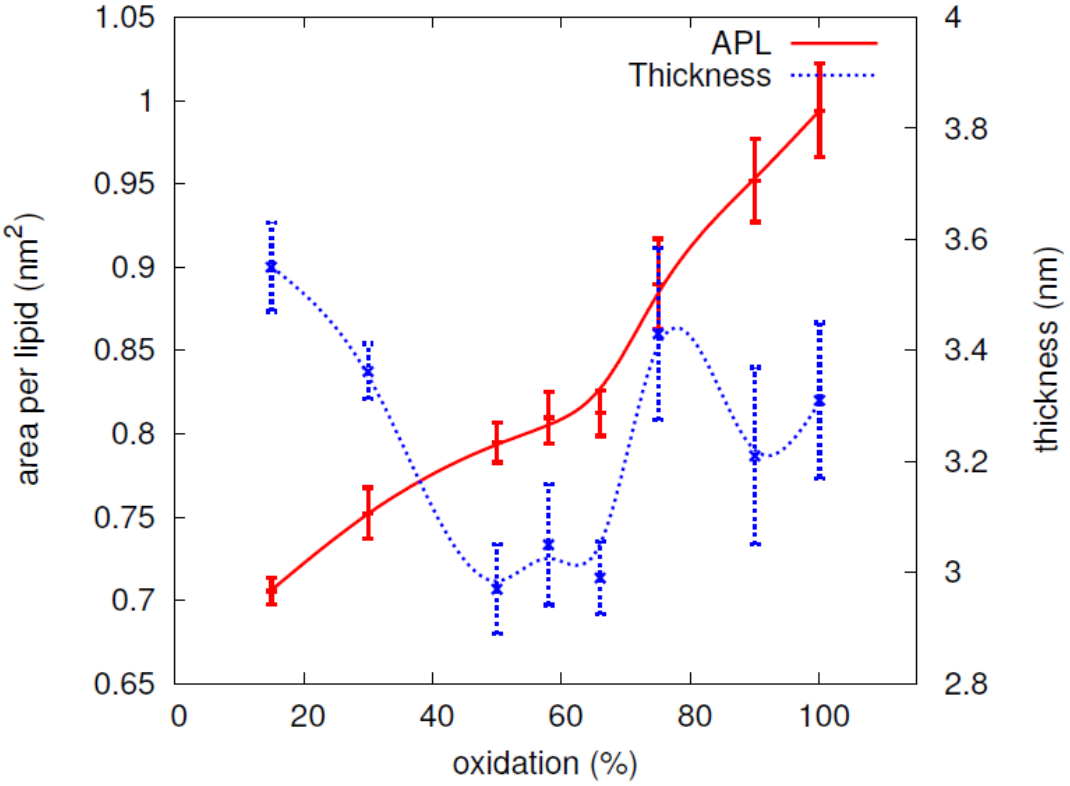

Figure 6. Average area per lipid and membrane thickness of the equilibrated membrane as a function of the degree of oxidation. The trailing 20 ns of MD trajectories were used for averaging, standard deviation is shown as errobars.

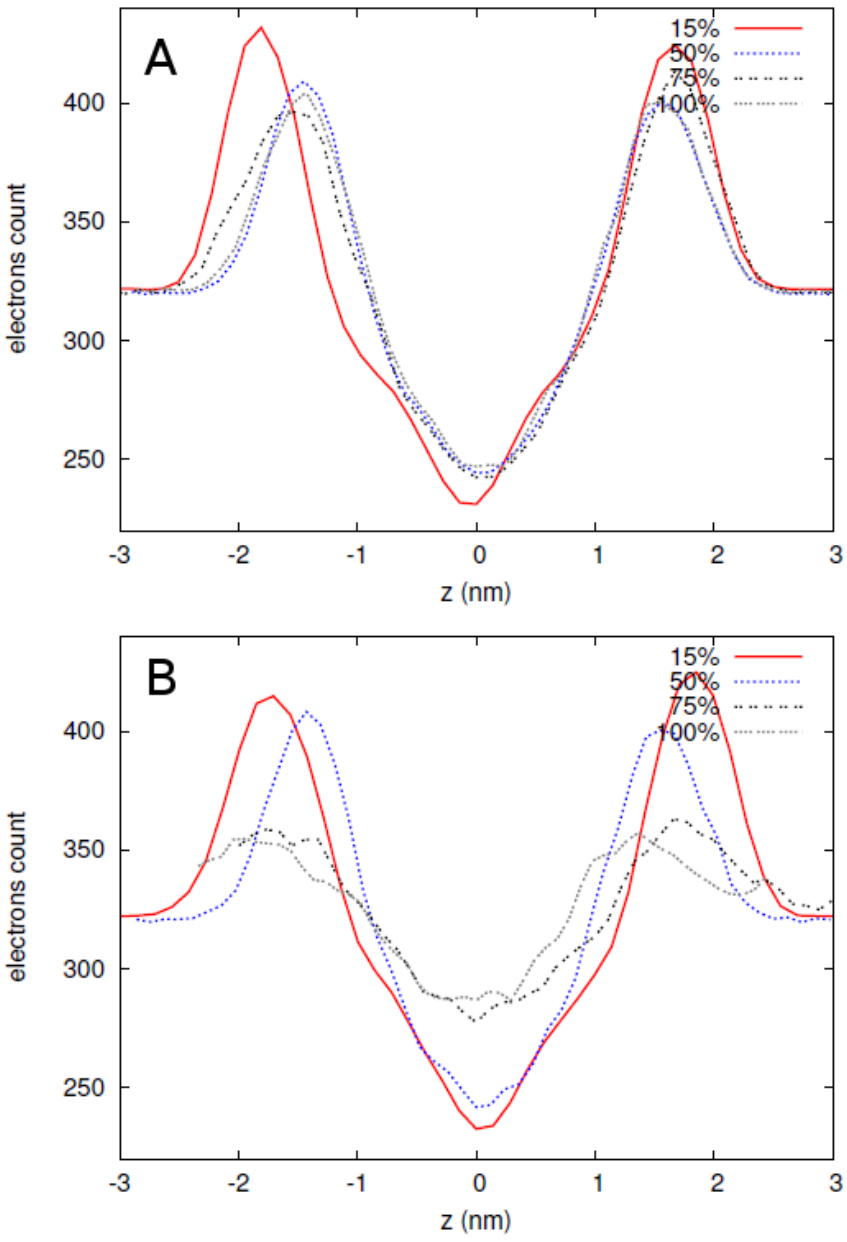

Figure 7. Density profiles for membranes with different degree of oxidation. The profiles calculated in the initial (A), and final (B) 10-ns sections of the MD trajectories are shown.

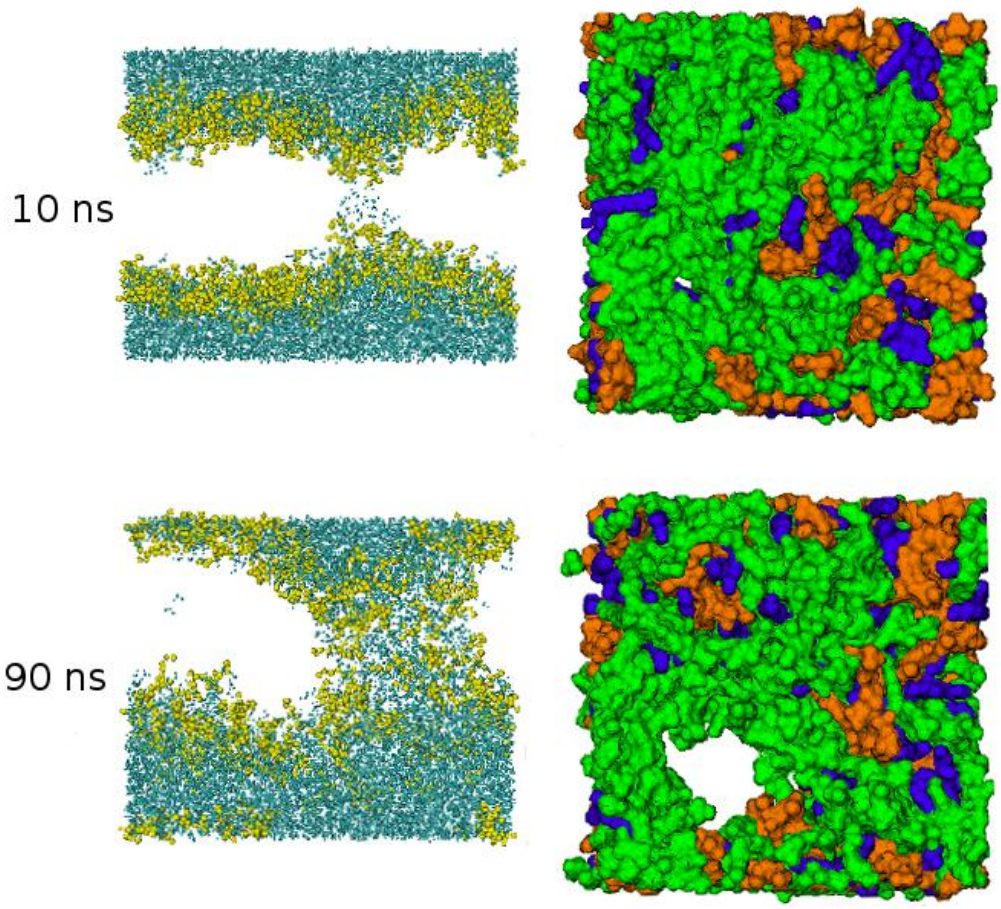

Figure 8. Snapshots of the simulation box for the system with 75% of oxidation taken at the initial (10 ns) and final (10 ns) stages of the MD trajectory. Side view (left column) and top view (right column) of the simulation box are presented. For clarity, only the phosphate groups of lipids are presented in the side view. Water molecules are removed from the top view. Color coding in the side views: water molecules – blue, lipid headgroups – yellow; top views: DOPC lipids – yellow, OX1PC – orange, nonanal – blue.

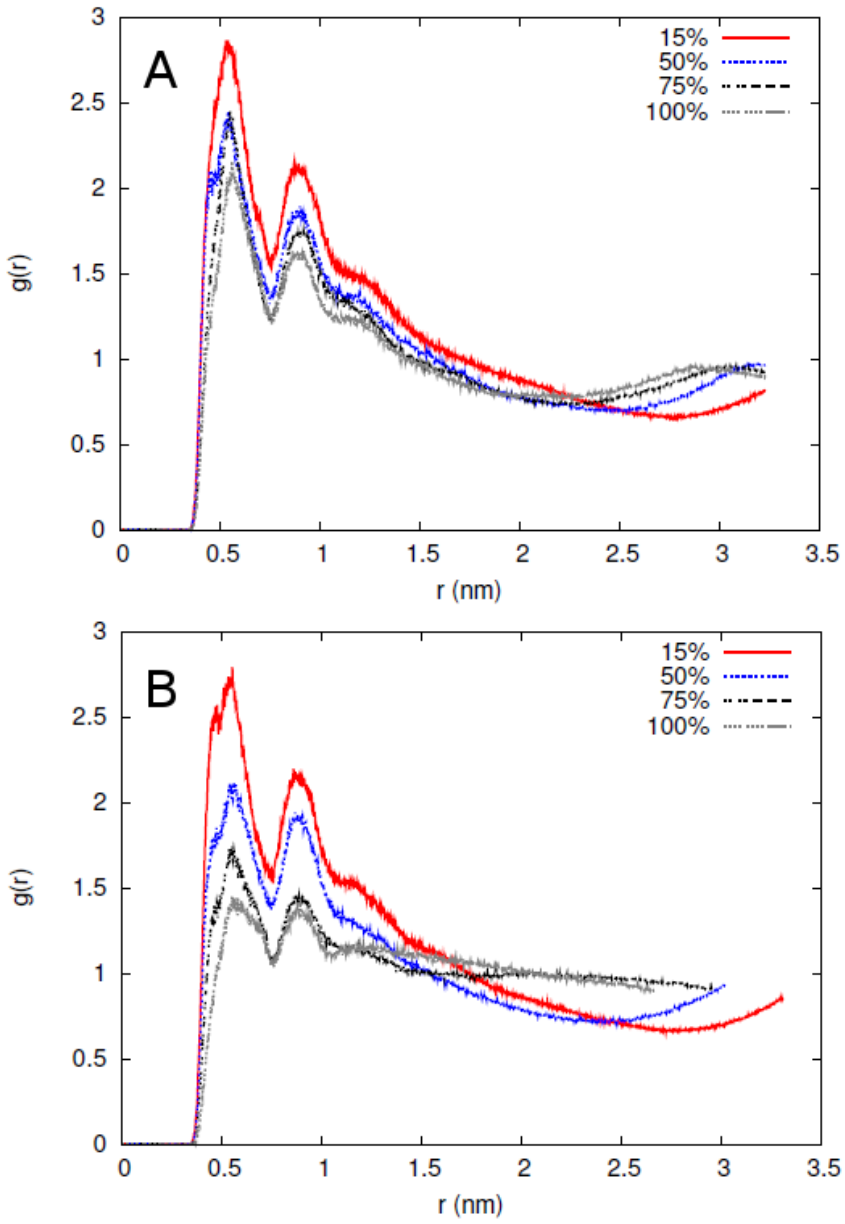

Figure 9. Radial distribution functions for phosphate–phosphate distances calculated in the initial (A), and final (B) 10-ns sections of the MD trajectories.

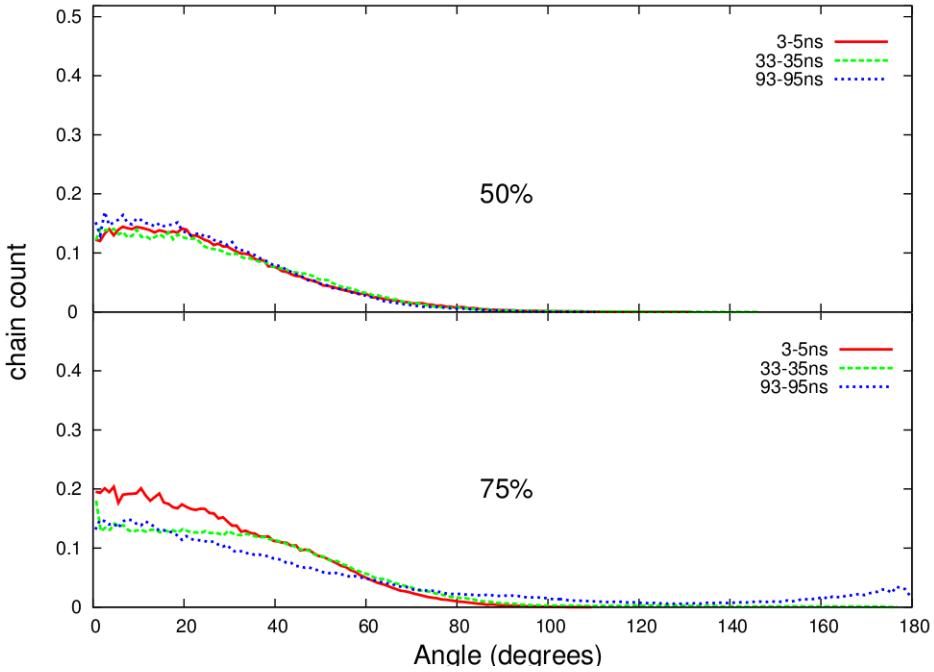

Figure 10. Distribution of angles between the oxidized chain (defined as a vector connecting the first carbon atom of the chain with the oxygen atom of the aldehyde group) and the normal to the bilayer for oxidized lipid molecules at different levels of oxidation. The data for systems with 50% (upper panel) and 75% (bottom panel) of oxidized lipids are shown; three stages of the MD simulations are presented. The angle of 0° corresponds to the orientation of a chain toward the membrane interior, whereas the value of 180° represents the chains entirely reoriented towards the water phase.

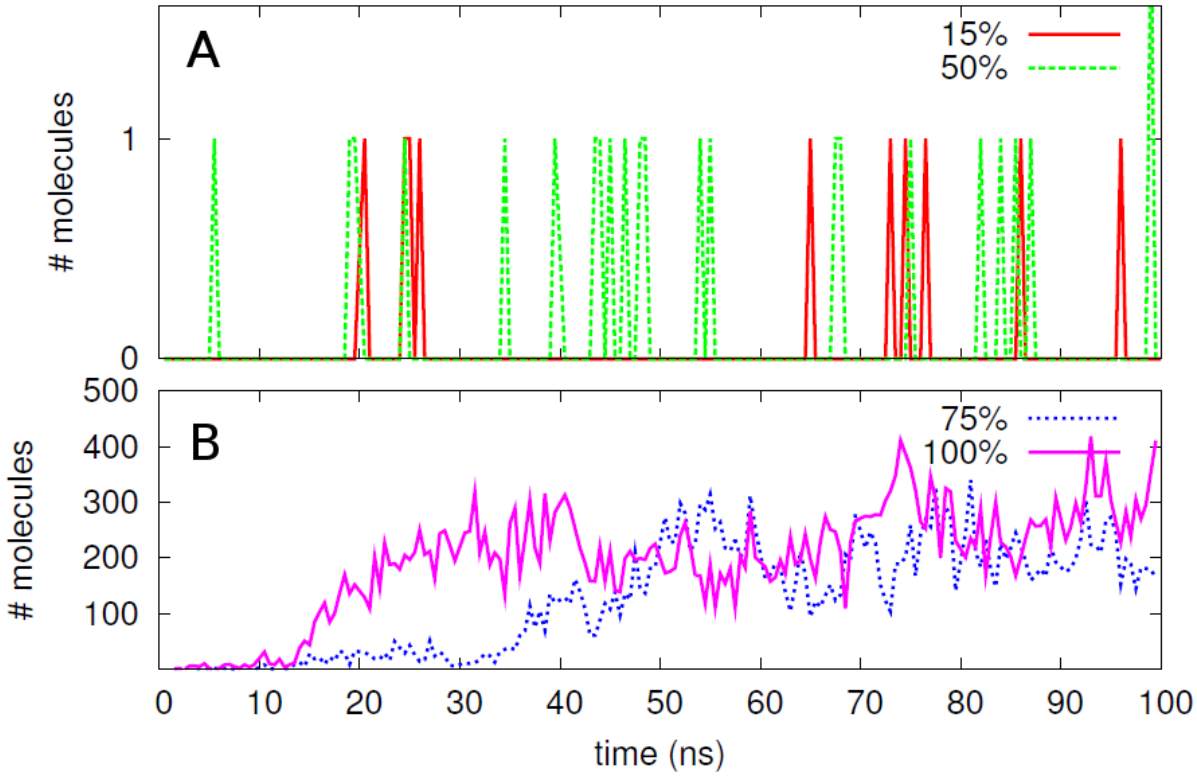

Figure. 11. Water permeation across the membrane (number of water molecules crossing the bilayer center) as a function of simulation time for moderately (A) and massively (B) oxidized membranes.

References

1 J. M. Berg, J. L. Tymoczko and L. Stryer, in *Biochemistry*, W. H. Freeman, New York, 2002.

2 D. W. Deamer and J. Bramhall, *Chemistry and Physics of Lipids*, 1986, **40**, 167-188.

3 S. Brambillasca, M. Yabal, P. Soffientini, S. Stefanovic, M. Makarow, R. S. Hegde and N. Borgese, *Embo Journal*, 2005, **24**, 2533-2542.

4 R. Volinsky, L. Cwiklik, P. Jurkiewicz, M. Hof, P. Jungwirth and P. K. J. Kinnunen, *"Oxidized phosphatidylcholines facilitate phospholipid flip-flop in liposomes", submitted*, 2011.

5 A. Gurtovenko and I. Vattulainen, *Biophysical journal*, 2007, **92**, 1878-1890.

6 S. J. Marrink, A. H. de Vries and D. P. Tieleman, *Biochimica Et Biophysica Acta-Biomembranes*, 2009, **1788**, 149-168.

7 A. A. Gurtovenko, J. Anwar and I. Vattulainen, *Chemical Reviews*, 2010, **110**, 6077-6103.

8 K. Gawrisch, H. C. Gaede, M. Mihailescu and S. H. White, *Eur. Biophys. J. Biophys. Lett.*, 2007, **36**, 281-291.

9 J. C. Weaver, *Journal of Cellular Biochemistry*, 1993, **51**, 426-435.

10 D. P. Tieleman, H. Leontiadou, A. E. Mark and S. J. Marrink, *Journal of the American Chemical Society*, 2003, **125**, 6382-6383.

11 L. Cwiklik and P. Jungwirth, *Chemical Physics Letters*, 2010, **486**, 99-103.

12 H.-P. Deigner and A. Hermetter, *Current opinion in lipidology*, 2008, **19**, 289-294.

13 G. O. Fruhwirth, A. Loidl and A. Hermetter, *Biochimica et biophysica acta*, 2007, **1772**, 718-736.

14 K. Sabatini, J. P. Mattila, F. M. Megli and P. K. J. Kinnunen, *Biophysical journal*, 2006, **90**, 4488-4499.

15 H. Khandelia and O. G. Mouritsen, *Biophysical journal*, 2009, **96**, 2734-2743.

16 J. Wong-Ekkabut, Z. Xu, W. Triampo, I. M. Tang, D. P. Tieleman and L. Monticelli, *Biophysical journal*, 2007, **93**, 4225-4236.

17 L. Beranova, L. Cwiklik, P. Jurkiewicz, M. Hof and P. Jungwirth, *Langmuir*, 2010, **26**, 6140-6144.

18 H. L. Smith, M. C. Howland, A. W. Szmodis, Q. Li, L. L. Daemen, A. N. Parikh and J. Majewski, *Journal of the American Chemical Society*, 2009, **131**, 3631-3638.
19 A. Pashkovskaya, E. Kotova, Y. Zorlu, F. Dumoulin, V. Ahsen, I. Agapov and Y. Antonenko, *Langmuir : the ACS journal of surfaces and colloids*, 2009.
20 M. J. Hope, M. B. Bally, G. Webb and P. R. Cullis, *Biochim Biophys Acta*, 1985, **812**, 55-65.
21 J. C. Mathai, S. Tristram-Nagle, J. F. Nagle and M. L. Zeidel, *J Gen Physiol*, 2008, **131**, 69-76.
22 M. Jansen and A. Blume, *Biopchys. J.*, 1995, **68**, 997-1008.
23 Y. Graziani and A. Livne, *J. Membrane Biol.*, 1972, **7**, 275-284.
24 Y. Graziani and A. Livne, *Biochim Biophys Acta*, 1973, **291**, 612-620.
25 J. F. Nagle and S. Tristram-Nagle, *Biochim. Biophys. Acta*, 2000, **1469**, 159-195.
26 M. Jansen and A. Blume, *Biophys J*, 1995, **68**, 997-1008.
27 J. Degier, *Chem Phys Lipids*, 1993, **64**, 187-196.
28 M. L. Fernandez, G. Marshall, F. Sagues and R. Reigada, *J Phys Chem B*, 2010, **114**, 6855-6865.
29 A. Gauthier and B. Joos, *J. Chem. Phys.*, 2007, **127**, 105104.
30 O. Berger, O. Edholm and F. Jahnig, *Biophysical Journal*, 1997, **72**, 2002-2013.
31 H. J. C. Berendsen, J. P. M. Postma, W. F. van Gunsteren and J. Hermans, in *Intermolecular Forces*, ed. B. Pullman, D. Reidel Publishing Company, Dordrecht, 1981, pp. 331-342.
32 S. Tristram-Nagle, H. I. Petrache and J. F. Nagle, *Biophys. J.*, 1998, **75**, 917-925.
33 M. Parrinello and A. Rahman, *Journal of Applied Physics*, 1981, **52**, 7182-7190.
34 T. Darden, D. York and L. Pedersen, *Journal of Chemical Physics*, 1993, **98**, 10089-10092.
35 S. Miyamoto and P. A. Kollman, *Journal of Computational Chemistry*, 1992, **13**, 952-962.
36 B. Hess, H. Bekker, H. J. C. Berendsen and J. Fraaije, *Journal of Computational Chemistry*, 1997, **18**, 1463-1472.
37 B. Hess, C. Kutzner, D. van der Spoel and E. Lindahl, *Journal of Chemical Theory and Computation*, 2008, **4**, 435-447.

38 J. K. Mills and D. Needham, *Bba-Biomembranes*, 2005, **1716**, 77-96.
39 M. Przybylo, K. Cyprych and M. Langner, *submitted*, 2011.
40 Y. Liu and J. Nagle, *Physical Review E*, 2004, **69**, 1-4.
41 E. Sackmann, in *Handbook of Biological Physics*, ed. R. Lipowsky and E. Sackmann, Elsevier Science B.V., 1995, vol. 1, pp. 1-62.
42 M. C. Hull, D. B. Sauer and J. S. Hovis, *J. Phys. Chem. B*, 2004, **108**, 15890-15895.
43 J. Alper, *Science*, 2002, **296**, 838-839.
44 E. M. Bevers, P. Comfurius, D. W. C. Dekkers, M. Harmsma and R. F. A. Zwall, *Biol. Chem.*, 1998, **379**, 973-986.
45 J. Davidsen, O. G. Mouritsen and K. Jorgensen, *Bba-Biomembranes*, 2002, **1564**, 256-262.
46 T. H. Haines, *Febs Lett*, 1994, **346**, 115-122.
47 G. R. Dubyak, *Adv. Physiol. Educ.*, 2004, **28**, 143-154.
48 F. X. Contreras, L. Sanchez-Magraner, A. Alonso and F. M. Goni, *Febs Lett*, 2010, **584**, 1779-1786.
49 D. L. Daleke, *J. Lipid Res.*, 2003, **44**, 233-242.
50 A. A. Gurtovenko and I. Vattulainen, *J. Phys. Chem. B*, 2007, **111**, 13554-13559.
51 A. Y. Mulkidjanian, J. Heberle and D. A. Cherepanov, *Biochim. Biophys. Acta*, 2006, **1757**, 913-930.
52 G. Benga, *Cell Biology International*, 2003, **27**, 701-709.
53 T. M. Allen, *Drugs*, 1997, **54**, 8-14.
54 Y. Barenholz, *Curr Opin Colloid & Interf. Sci*, 2001, **6**, 66-77.
55 V. Centis and P. Vermette, *Colloids Surf. B; Biointerfaces*, 2008, **65**, 239-246.
56 M. L. Chen, *Adv Drug Deliv Rev*, 2008, **60**, 768-777.
57 K. A. Edwards and A. J. Baeumner, *Talanta*, 2006, **68**, 1432-1441.
58 A. Fritze, F. Hans, A. Kimpfler, R. Schubert and R. Peschka-Suss, *Biochi Biophys Acta*, 2006, **1758**, 1633-1640.

59 A. Gomez-Hens and J. M. Fernandez-Romero, *Trends Analyt. Chem.*, 2006, **25**, 167-178.